A RED SUPERGIANT NEBULA AT 25 MICRON: ARCSECOND SCALE MASS-LOSS ASYMMETRIES OF μ CEP[1]

W.J. DE WIT[2], R.D. OUDMAIJER[2], T. FUJIYOSHI[3], M.G. HOARE[2], M. HONDA[4], H. KATAZA[5], T. MIYATA[6], Y. K. OKAMOTO[7], T. ONAKA[8], S. SAKO[6], T. YAMASHITA[3]

ABSTRACT

We present diffraction limited (0.6″) 24.5 μm Subaru/COMICS images of the red supergiant μ Cep. We report the detection of a circumstellar nebula, that was not detected at shorter wavelengths. It extends to a radius of at least 6″ in the thermal infrared. On these angular scales, the nebula is roughly spherical, in contrast, it displays a pronounced asymmetric morphology closer in. We simultaneously model the azimuthally averaged intensity profile of the nebula and the observed spectral energy distribution (SED) using spherical dust radiative transfer models. The models indicate a constant mass-loss process over the past 1000 years, for mass-loss rates a few times 10^{-7} M$_\odot$ yr^{-1}. This work supports the idea that at least part of the asymmetries in shells of evolved massive stars and supernovae may be due to the mass-loss process in the red supergiant phase.

Subject headings: (stars:) supergiants - stars: evolution - stars : individual μ Cep - stars: mass-loss

1. INTRODUCTION

Although the final stages of the post-main sequence evolution of massive stars do not last long, it is here where most of the mass is lost and the shaping of the pre-supernova ejecta takes place. Key in this respect are the Red Supergiants (RSGs) which represent a phase in the life of stars with initial masses 10–30 M$_\odot$. During this phase lasting $10^4 - 10^5$ years, the stars lose prodigious amounts of mass at a rate of order $10^{-6} - 10^{-4}$ M$_\odot$ yr^{-1} (van Loon et al. 2005; Massey et al. 2008), and the final mass of the objects is mostly set during this phase. RSGs have been observed to be the direct progenitors of Type IIP supernovae (Smartt et al. 2004), but can also evolve towards the blue via a Yellow Hypergiant phase (Oudmaijer et al. 2008; de Wit et al. 2008a) to become a Wolf-Rayet star and eventually explode as a supernova (Meynet & Maeder 2000).

It is not only the study of the stars themselves that helps us understand the final stages of the evolution of massive stars. Investigating RSGs' mass-loss and their circumstellar material helps us to understand the origin of the aspherical structures found around supernovae, such as SN 1987A's rings, or gamma-ray bursts. It is possible that at least some of these observed asymmetries originate during the RSG phase (e.g. Chita et al. 2008). Indeed, in several instances, the mass-loss during the RSG phase has been found to deviate from spherically symmetric, and can have a complex appearance. Much effort has been directed towards the objects VY

CMa and NML Cyg, extremely bright, cool, objects close the empirical Humphreys Davidson limit (Humphreys & Davidson 1979). High resolution studies have revealed highly anisotropic structures in the wind of VY CMa (e.g. Smith et al. 2001), while NML Cyg's aspherical appearance is shaped by the strong radiation from the nearby Cyg OB2 association (Morris and Jura 1983; Schuster et al 2006).

A third RSG that is found in the same location in the HR diagram as the above two objects is μ Cep (Schuster et al 2006). Contrary to these two cooler objects, little is known about the material surrounding μ Cep. This can be readily explained by its mass-loss, which is orders of magnitude lower than for NML Cyg or VY CMa (cf. Jura & Kleinman 1990). With an $M_{\rm bol}$ of -9.08, this M2Ia star is one of the brightest RSGs known, lying on evolutionary tracks corresponding to stars with initial masses greater than 25 M$_\odot$ (Levesque et al. 2005). Using Levesque et al.'s parameters, we find a distance to the object of 870 pc, and a luminosity of $\sim 3\times10^5$ L$_\odot$. Here, we report on the discovery of an extended dust shell around the object by means of diffraction limited imaging (0.6″) of mid-IR thermal dust emission.

2. OBSERVATIONS AND DATA REDUCTION

μ Cep was observed on 6 different occasions as a mid-IR standard star between June 2003 and July 2004 with the COMICS instrument mounted on the 8.2 meter Subaru telescope in Hawaii (Kataza et al. 2000; Okamoto et al. 2003; Sako et al. 2003). The star was imaged using the Q24.5-OLD and Q24.5-NEW filters both centred on 24.5 μm. The imaging mode of COMICS utilises a Raytheon 320×240 Si:As IBC array with a pixel scale of 0.13″. This scale comfortably samples the diffraction limit for the 8.2m Subaru telescope at this wavelength, which is 0.6″. The observations are summarised in table 1. More details on the filters and data reduction can be found in de Wit et al. (2008b, in prep.).

μ Cep is bright and therefore often used as a standard star, either for determining the instrumental point-spread-function (PSF) or for calibrating photometry. We observed the object for calibration purposes for a different project (as reported in de Wit et al. 2008b), and found that it was extended compared to other PSF reference stars. As μ Cep was the PSF standard, we do not have a concomitant PSF reference observations. However, we can use as a reference PSF the remaining three

---

[1] Based on data collected at the Subaru telescope, which is operated by the National Astronomical Observatory of Japan.

[2] School of Physics & Astronomy, University of Leeds, Woodhouse Lane, Leeds LS2 9JT, UK; w.j.m.dewit@leeds.ac.uk

[3] Subaru Telescope, National Astronomical Observatory of Japan, National Institutes of Natural Sciences, 650 North A'ohoku Place, Hilo, HI 96720, USA

[4] Department of Information Science, Kanagawa University, 2946 Tsuchiya, Hiratsuka, Kanagawa, 259-1293, Japan

[5] Department of Infrared Astrophysics, Institute of Space and Astronautical Science, Japan Aerospace Exploration Agency, Sagamihara, Kanagawa, 229-8510, Japan

[6] Institute of Astronomy, University of Tokyo, Osawa 2-21-1, Mitaka, Tokyo 181-0015, Japan

[7] Faculty of Science, Ibaraki University, 2-1-1 Bunkyo, Mito, Ibaraki, 310-8512, Japan

[8] Department of Astronomy, Graduate School of Science, University of Tokyo, Bunkyo-ku, Tokyo 113-0022, Japan
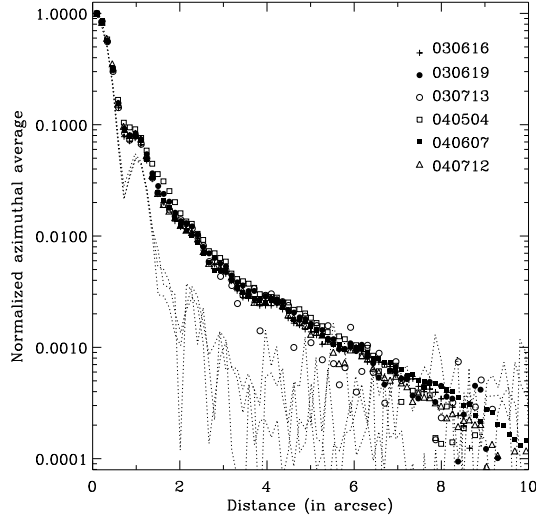
Fig. 1.— The azimuthally averaged and normalized intensity profile of μ Cep as observed at 6 different dates. The profile is stable. Note the slightly narrower profile for the 030713 data. These are less sensitive, and with a SNR a factor of 10 less than the other data, the faint outer parts can not be measured. Also shown are the intensity profiles of the 3 genuine PSF objects. Note the first two Airy rings at ~ 1.2″ and ~ 2.4″.

genuine PSF objects observed for the same project: α Tau and asteroids 51 and 511. To illustrate the stability of the observational set-up and the extent of μ Cep, we show in Fig. 1 the, azimuthally averaged, normalized intensity profiles of the 3 genuine PSF standards and those of each of the 6 observations of μ Cep. The 3 point sources have virtually identical profiles, and the noise begins to dominate only after ~4″. On the contrary, the profiles for μ Cep are clearly extended with respect to the 3 PSF standards to at least 6″, and they are also hardly different from each other on all occasions. The lowest signal-to-noise ratio (SNR) data of μ Cep (taken in July 2003) also reveal that the object is extended, but the data are not deep enough to probe the extent as well as the higher SNR data. We conclude that μ Cep is extended at 24.5 μm.

3. RESULTS

3.1. *The 24.5 μm images: asymmetric dust distribution*

The highest SNR image (taken on 04/06/07) of μ Cep is shown in the left panel of Fig. 2. We have subtracted from this image the scaled profile of the PSF standard asteroid 511 in order to enhance the features of μ Cep's circumstellar emission. For comparison we show in the right panel of Fig. 2 the PSF standard α Tau with again a PSF profile subtracted. It is clear that μ Cep has extended circumstellar emission reaching distances from the star of at least 6″. The outer parts of the shell-like structure are roughly circular with indications of larger scale inhomogeneities. In contrast, the inner parts reveal a clearly asymmetric, bipolar type, geometry at a position angle of ~67°. The elliptical structure is visible from the inner parts and extends to 2.2″ along the major axis on either side of the central star, and 1.4″ along the minor axis. The intensity contrast between the brighter regions and the fainter regions at the same distance from the star is a factor of 2.

3.2. *Dust radiative transfer modelling*

Emission at 24.5 μm stays optically thin for large columns of dust. Resolved images allow us to simultaneously model the dust emission as a function of distance from the star (the

intensity profile) and the total dust emission as given by the SED. For this purpose, we employ DUSTY, a code that solves self-consistently the scaled 1D dust radiative transfer problem (see Ivezić & Elitzur 1997). We use a spherically symmetric dust distribution, that is illuminated by a central, unresolved star. Its radiation is represented by a Kurucz ATLAS9 atmosphere model (Kurucz 1993) with $T_{\rm eff}$ = 3750 K, solar metallicity and surface gravity corresponding to the supergiant nature of μ Cep, i.e. log(g) = 0.0. We use oxygen-rich dust with a condensation temperature of 1000 K. The dust particles follow a MRN size distribution (Mathis, Rumple, & Nordsieck 1977). Within the limitation of a spherical model, we experiment with (1) the amount of dust as parametrized by the total optical depth A_V; (2) the radial density distribution of the dust $\propto r^{-p}$, adopting a constant ($p = 2$) or declining ($p = 1.5$) mass-loss rate; (3) two different silicate opacity tables, the ones provided by Draine & Lee (1984) and for "warm" silicates by Ossenkopf et al. (1992). The outer bound of the model is set at 1000 times the dust condensation radius, but the exact value is of little influence on the total excess flux at wavelengths shortward of ~25 μm as long as the outer radius is much larger than the inner dust condensation radius.

We build μ Cep's SED using a mid-IR spectrum taken with the short wavelength spectrometer (SWS, de Graauw et al. 1996) on board the ISO satellite (Kessler et al. 1996), near-IR *JHKLM* photometry from Heske (1990) and visual broadband *UBVRI* Johnson photometry from Lee (1970). The photometry is dereddened for an interstellar extinction of $A_V = 1.5^m$ (Levesque et al. 2005). The IRAS 60 μm and 100 μm data points lie above the extrapolated ISO-SWS spectrum. This excess flux is due to the much larger beam of IRAS and comes from extended cool dust emission. The origin of this emission is not obvious, it could be either due to the interstellar medium being heated up by the stellar radiation (cf. Oudmaijer 1996), or a very extended shell which is the result of a previous mass-loss phase (e.g. Stencel et al. 1988). It should be kept in mind that we only consider the most recent mass-loss episode here.

The fit procedure initially estimates the $L_{\rm bol}$ by matching the overall shape of the scaled model SED to the observed one. DUSTY's output images are then accordingly scaled and convolved with the instrumental PSF. A comparison of model infrared excess and model intensity profile to the observed ones is made for all generated models. A simple tally is performed based on a goodness-of-fit criterion. The model that fits both sets of data best is the one with the highest average ranking in the two tallies.

The results of the 1D modelling are presented in Fig. 3. Once the intensity profile is fit for a given nebular structure and stellar luminosity, the SED can be matched by increasing the amount of dust in the given nebula. The normalized intensity profile is quite insensitive to the total amount of dust for small optical depths. We chose to prioritize a fit to the slope of the continuum longward of the silicate feature rather than the silicate emission profile. Details for each of the three models presented in Fig. 3 are given in Table 1. We present the two best-fitting $p = 2$ models corresponding to the two different silicate opacities. The silicate emission feature is not well matched by either model, although the intensity profile is better fit by model #1 (full line). At the inner 2″ the models predict too much intensity, which is consistent with a deviation from spherical symmetry seen in the images. Models with a shallow $p = 1.5$ radial density profile fit the intensity profile worst as is illustrated by model #3. This demonstrates the
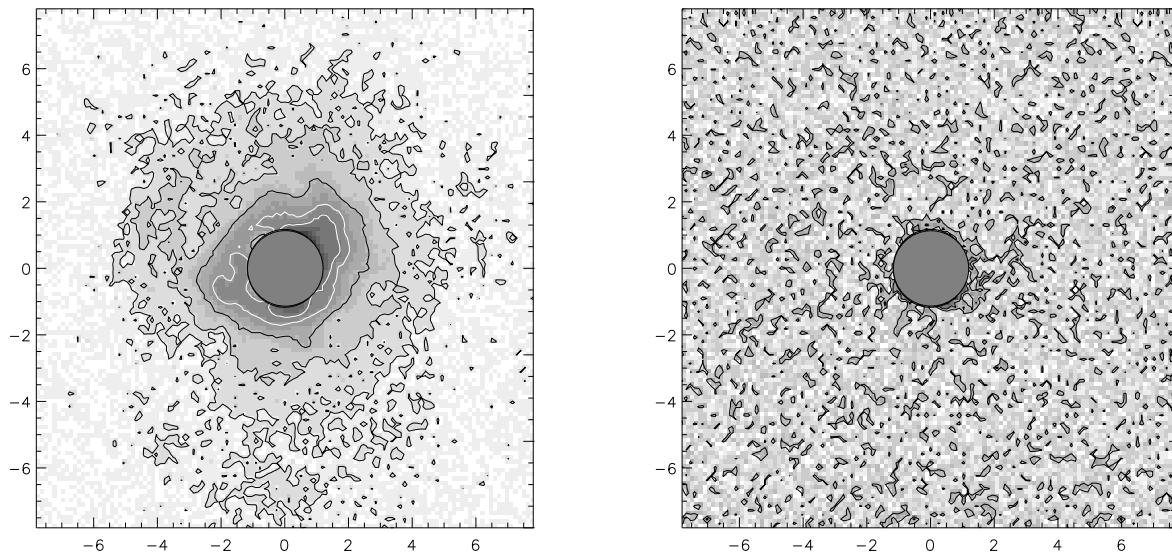
Fig. 2.— The PSF subtracted image of μ Cep (left) and the PSF standard α Tau (right). The instrumental PSF was determined from the point source asteroid 511. The region within 1.2″ is masked to hide artefacts from the subtraction procedure. μ Cep is clearly extended, and an asymmetry originates from close to the star. The contour levels are chosen to enhance the contrast between the intensity levels, lowest contour corresponds to twice the standard deviation in the background level. North is to the left, East is to the bottom.

value of spatial information in this type of analysis, because the SED is at the same time very well matched by model #3. All models have a mass-loss rate of a few $10^{-7}\,\mathrm{M_\odot\,yr^{-1}}$ for an expansion velocity of $10\,\mathrm{km\,s^{-1}}$ (cf. Le Borgne & Mauron 1989).

4. DISCUSSION

We have presented the first high-resolution (0.6″) images of the circumstellar environment of the RSG μ Cep. This material has not been seen in previous imaging campaigns. For a sample of massive evolved objects, Schuster et al. (2006) obtained deep optical images with the HST to search for scattered light by circumstellar dust. They detected only those sources which have mass-loss rates many orders of magnitude larger than μ Cep over the past 500–1000 years. Le Borgne & Mauron (1989) searched for optical, reflected emission in their polarization data. These authors made pointed observations with a 10″ diaphragm at several locations around the star and detected (faint) polarized light as far as 20″ from the star. Other evidence for extended emission comes from Mauron (1997), who finds resonance scattered K I line emission at distances further than 20″ from the star. These data were taken at 2 slit positions, and thus do not allow for conclusive statements about the geometry of the circumstellar matter to be made. They do appear to indicate the presence of either clumpy material or several discrete mass-loss episodes in the recent past. The data presented in this paper traces material out to 6″. As an expansion velocity of $10\,\mathrm{km\,s^{-1}}$ at a distance of 1 kpc corresponds to about 1″ per 500 yr, the mass lost 2000–3000 years ago appears to have been ejected in a roughly spherically symmetric way. However, the most recent mass lost, ejected less than 1000 years ago, shows a pronounced axisymmetric geometry in our high resolution images.

One may speculate whether this geometry is due to a bipolar flow colliding with the spherically symmetric previous wind, or a slowly expanding torus. It is useful in this respect to consider the current findings for the more numerous lower-mass counterparts of RSGs, the Asymptotic Giant Branch (AGB)

TABLE 1
INPUT PARAMETERS AND DERIVED QUANTITIES OF THE MODELS PRESENTED IN FIG 3. DL AND OW DUST TYPES STAND FOR DRAINE & LEE (1984), AND OSSENKOPF ET AL. (1992) SILICATES. MODEL #1 IS THE PREFERRED MODEL.

#	p	R_{in} (mas)	R_{out}/R_{in}	L ($L_\odot$)	dust	A_V	M_{dust} ($M_\odot$)	$\dot{M}$ ($\mathrm{M_\odot\,yr^{-1}}$)
1	2.0	75	$1\,10^3$	$3.3\,10^5$	DL	0.70	$1.4\,10^{-2}$	$4.5\,10^{-7}$
2	2.0	103	$1\,10^3$	$3.1\,10^5$	OW	0.60	$2.2\,10^{-2}$	$5.2\,10^{-7}$
3	1.5	112	$1\,10^2$	$3.9\,10^5$	OW	0.30	$5.0\,10^{-3}$	$1.6\,10^{-7}$

stars. Data on these are also sparse, but asymmetries of the circumstellar material have been seen at high-resolution in several cases (e.g. Menut et al. 2007 and Murakawa et al. 2005 for IRC +10216; Vinković et al. 2004 and Inomata et al. 2007 for IRC +10011). The picture that emerges from such individual studies is that the outer parts of the AGB stars are fairly spherical. The inner parts are relatively complex, and can be best explained with a torus type structure close to the star, perhaps carved out by a bi-polar flow. Based on a compilation of the best data available, Huggins (2007) finds that, in general, tori correspond to low outflow velocities and jets with higher speeds, in excess of $100\,\mathrm{km\,s^{-1}}$. In addition, he concludes that the jets develop shortly after a torus is ejected. Given that the CO spectra of μ Cep indicate low velocities rather than high velocities, it is very well possible that we are now witnessing the same for a Red Supergiant.

5. CONCLUDING REMARKS

We have obtained the first diffraction-limited images of a Red Supergiant at $24.5\,\mu$m, and resolved the circumstellar material around μ Cep out to 6″. The intensity profile and the SED were simultaneously fitted with a dust model. The main results can be summarized as follows:

1. The outer parts of the shell are to first order circular with apparent inhomogeneities, the inner parts, tracing the mass lost in the past 1000 years display a flattened structure, which is possibly a slowly expanding, dense torus. The immediate
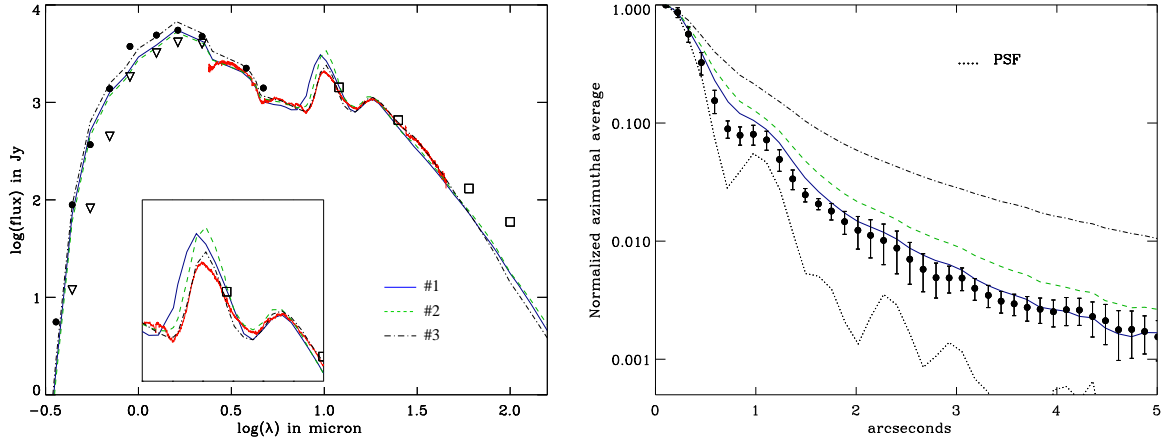
Fɪɢ. 3.— Model fits to the SED (left panel) and the 24.5 μm intensity profile (right panel). Three models are shown corresponding to the parameters given in Table 2. Filled circles represent the extinction corrected optical and near-IR data (open triangles). Sources of the SED data are discussed in the text.

conclusion from this is that any asymmetries in the shells of massive evolved stars and Supernovae ejecta may find their origins in the Red Supergiant phase. This is qualitatively very similar to what is found for the lower-mass AGB stars which evolve into bipolar Planetary Nebulae.

2. The mass-loss rate for μ Cep is found to be a few times $10^{-7}\,M_\odot\,yr^{-1}$. This low mass-loss rate may explain the fact that μ Cep is not detected in scattered light, as opposed to other RSGs which have mass-loss rates that are orders of magnitude larger.

3. A general conclusion is that imaging thermal dust emission at 24.5 μm is a viable manner to spatially resolve the circumstellar material around evolved objects with low mass-

loss rates and as a consequence are otherwise not detected with maser observations, CO imaging or scattered light imaging.

REFERENCES

de Graauw, T., Haser, L. N., Beintema, D. A., et al. 1996, A&A, 315, L49
Chita, S. M. and Langer, N. and van Marle, A. J. and García-Segura, G. and Heger, A., 2008, ArXiV 0807.3049
de Wit, W. J., Oudmaijer, R. D., Groenewegen, M. A. T., Hoare, M. G., & Malbet, F. 2008a, A&A, 480, 149
de Wit, W. J., Hoare, M. G., Fujiyoshi, T., Oudmaijer, R. D., Honda, M., Kataza, H., Miyata, T., K. Okamoto, Y., Onaka, T., Sako, S., Yamashita, T. 2008b, A&A, subm.
Draine, B. T. & Lee, H. M. 1984, ApJ, 285, 89
Heske, A. 1990, A&A, 229, 494
Huggins, P. J. 2007, ApJ, 663, 342
Humphreys, R. M. & Davidson, K. 1979, ApJ, 232, 409
Inomata, N., Imai, H., & Omodaka, T. 2007, PASJ, 59, 799
Ivezić, Z. & Elitzur, M. 1997, MNRAS, 287, 799
Jura, M. & Kleinmann, S. G. 1990, ApJS, 73, 769
Kataza, H., Okamoto, Y., Takubo, S., et al. 2000, in SPIE, Vol. 4008, eds. M. Iye & A. F. M. Moorwood, 1144
Kessler, M. F., Steinz, J. A., Anderegg, M. E., et al. 1996, A&A, 315, L27
Kurucz, R. L. 1993, VizieR Online Data Catalog, 6039
Le Borgne, J. F. & Mauron, N. 1989, A&A, 210, 198
Lee, T. A. 1970, PASP, 82, 765
Levesque, E. M., Massey, P., Olsen, K. A. G., et al. 2005, ApJ, 628, 973
Massey, P., Levesque, E. M., Plez, B., & Olsen, K. A. G. 2008, ArXiv e-prints, 0801.1806

Mathis, J. S., Rumpl, W., & Nordsieck, K. H. 1977, ApJ, 217, 425
Mauron, N. 1997, A&A, 326, 300
Menut, J.-L., Gendron, E., Schartmann, M., et al. 2007, MNRAS, 376, L6
Meynet, G. & Maeder, A. 2000, A&A, 361, 101
Morris, M. and Jura, M., 1983, ApJ 267, 179
Murakawa, K., Suto, H., Oya, S., et al. 2005, A&A, 436, 601
Okamoto, Y. K., Kataza, H., Yamashita, T., et al. 2003, in SPIE, Vol. 4841, eds. M. Iye & A. F. M. Moorwood, 169
Ossenkopf, V., Henning, T., & Mathis, J. S. 1992, A&A, 261, 567
Oudmaijer R.D. 1996, A&A 306, 823
Oudmaijer, R. D., Davies, B., de Wit, W.-J., & Patel, M. 2008, ArXiv e-prints, 0801.2315
Sako, S., Kataza, H., Miyata, T., et al. 2003, in SPIE, Vol. 4841, eds. M. Iye & A. F. M. Moorwood, 1211
Schuster, M. T., Humphreys, R. M., & Marengo, M. 2006, AJ, 131, 603
Smartt, S. J., Maund, J. R., Hendry, M. A., et al. 2004, Science, 303, 499
Smith, N., Humphreys, R. M., Davidson, K., et al. 2001, AJ, 121, 1111
Stencel, R. E. and Pesce, J. E. and Hagen Bauer, W. 1988, AJ,95, 141
van Loon, J. T., Cioni, M.-R. L., Zijlstra, A. A., & Loup, C. 2005, A&A, 438, 273
Vinković, D., Blöcker, T., Hofmann, K.-H., Elitzur, M., & Weigelt, G. 2004, MNRAS, 352, 852